# Measurements of liquid film thickness of a wide horizontal co-current stratified air-water flow

François Touron, Larbi Labraga, Laurent Keirsbulck, Hervé Bratec

▶ **To cite this version:**

François Touron, Larbi Labraga, Laurent Keirsbulck, Hervé Bratec. Measurements of liquid film thickness of a wide horizontal co-current stratified air-water flow. Thermal Science, 2015, 19 (2), pp.521-530. ⟨10.2298/TSCI120602212T⟩. ⟨hal-03452006⟩

**HAL Id: hal-03452006**

**https://uphf.hal.science/hal-03452006v1**

Submitted on 15 Apr 2022

**HAL** is a multi-disciplinary open access archive for the deposit and dissemination of scientific research documents, whether they are published or not. The documents may come from teaching and research institutions in France or abroad, or from public or private research centers.

L'archive ouverte pluridisciplinaire **HAL**, est destinée au dépôt et à la diffusion de documents scientifiques de niveau recherche, publiés ou non, émanant des établissements d'enseignement et de recherche français ou étrangers, des laboratoires publics ou privés.

Distributed under a Creative Commons CC BY-NC-ND 4.0 - Attribution - Non-commercial use - No Derivative Works - International License

# MEASUREMENTS OF LIQUID FILM THICKNESS OF A WIDE HORIZONTAL CO-CURRENT STRATIFIED AIR-WATER FLOW

by

***Francois TOURON*** [a], ***Larbi LABRAGA*** [a],
***Laurent KEIRSBULCK*** [a], ***and Herve BRATEC*** [b]

[a] University of Lille Nord de France, Lille, France; UVHC, TEMPO, Valenciennes, France
[b] Robert Bosch Produktie N. V., Tienen, Belgium

Original scientific paper
DOI: 10.2298/TSCI120602212T

*A horizontal co-current stratified two-phase flow was studied in a duct with a rectangular section. Its dimensions were such that the top and side walls did not influence the interfacial waves. The film thickness was almost of the millimeter. The Reynolds number based on the mean height and velocity in each phase varied from 0 to $1.16 \cdot 10^5$ in air and from 69 to 271 in water. These experimental conditions allowed the observation of the smooth, 2-D wavy and 3-D wavy stratified flow patterns. The interfacial waves were instantaneously measured on a 100 mm long line segment in the longitudinal midspan plane of the channel with the Level Detection and Recording technique. These measurements yielded statistical characteristics and highlighted the spectral differences between the 2-D and 3-D wavy stratified flow patterns.*

Key words: *two-phase flow, liquid film, wave*

## Introduction

Horizontal co-current stratified two-phase flows with thin liquid layer are at the center of various industrial processes, such as the cooling of fusion reactors, boilers, condensers, or gas absorption/desorption. In all these applications, the variation of mean film thickness and the mixing due to interfacial waves are known to strongly affect heat and mass transfers. Therefore, the characteristics of the liquid film are crucial data in many industrial problems. Extensive research has been done about stratified flows in horizontal pipes [1-3], in horizontal ducts of rectangular section with small dimensions (see for instance [4]), and about liquid free down flows [5]. Few studies presented interface measurements where the influence of the side and top walls of the duct could be neglected, the liquid layer was around a millimeter, and the gas stream was in the turbulent regime. Nevertheless, this configuration is of particular interest because it allows to focus on interfacial phenomena without interference. Besides, a low dependency on the geometry of the channel is ideal for the validation of a CFD code.

The purpose of this paper is to provide experimental data of the interface fluctuations for a water film in a horizontal duct of rectangular section and wide dimensions. First, we present the two-phase flow channel of the TEMPO laboratory. Then we describe our non-intrusive measurement technique. This technique visualizes the instantaneous shape of the interface in a

* Corresponding author; e-mail: francois.touron@gmail.com

vertical plane, and measures its level via image processing. Its accuracy is controlled with smooth stratified flows for which the balance equations can be solved. Finally, various statistical and spectral characteristics of the interface are discussed.

## Experiment

### *Experimental apparatus*

A diagram of the apparatus set-up for the air-water stratified two-phase flow experiment is given in fig. 1. The experiment was conducted in a horizontal channel with a rectangular section made of 20 mm thick transparent plexiglas planks. This channel was 3675 mm long and its internal dimensions were 200 mm wide and 140 mm high. At the inlet, the water injector was designed so that water came homogeneously and in smooth contact with air. After flowing through the channel, the water was stopped by a low fence and driven by gravity to a tank. A centrifugal pump was used to set water into motion in the open-loop circuit. The flow rate of the water was regulated by a manual valve and controlled visually with a rotameter. A 11 kW centrifugal fan controlled with a variable-frequency drive allowed to reach a streamwise velocity of 13 m/s. The experiment was conducted at near atmospheric pressure and room temperature.

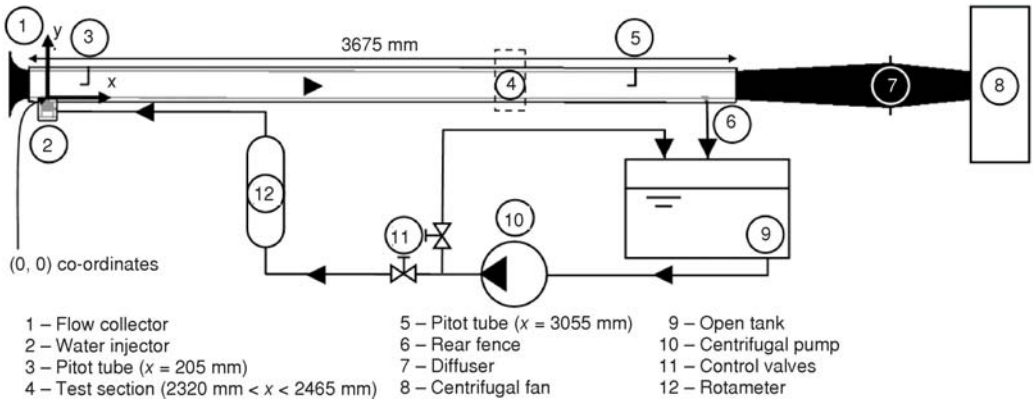


**Figure 1. Experimental apparatus**

In order to assess the quality of the flow, laser Doppler velocimetry was used in the test section for two different air velocities and without water. Streamwise velocity profiles were obtained in the midspan plane at 2462 mm from the inlet, they follow the universal profile of fully developed turbulent boundary layers. Besides, the top and bottom boundary layers are separated from each other, ensuring a limited influence of the top wall in the case of a co-current stratified two-phase flow with low holdup $\alpha$.

### *Level detection and recording (LeDaR) technique*

Measurements of the film thickness were made in the midspan plane of the test section. We used a technique initially developed at the von Karman Institute called the LeDaR [6-8]. As sketched in fig. 2, this technique relies on a CCD camera synchronized to a laser sheet to record images of the illuminated interface. With a liquid appropriately seeded with a fluorescent dye, the interface appears as a curve of high luminous intensity. In this study, a CCD camera TSI PowerView 4M Plus with resolution 2048 × 2048 px was placed on the side of the channel, with

a 105 mm objective and no filter. It allowed to record the interface for $x \in$[2320 mm, 2420 mm], while maintaining a spatial resolution of 0.053 mm/px. The laser sheet was produced with a pulsed Nd:YAG laser (Quantel, Twins BSL 200) of wavelength 532 nm. The axis of the camera was not set exactly perpendicular to the laser sheet but rather slightly plunging, so that 3-D waves did not distort the luminous line appearing at the interface. An angle of 10° was found to be a good compromise so as to keep a good vertical resolution. The water was seeded with fluorescein diluted at 0.1 g/L.

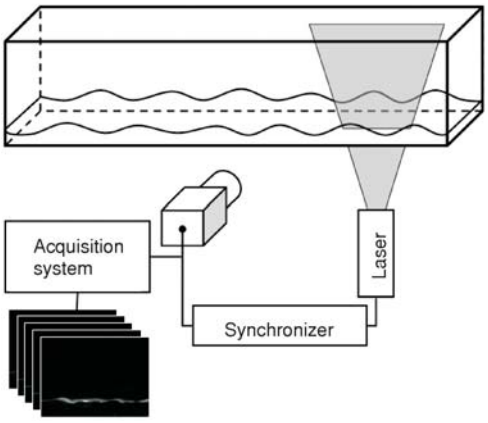


**Figure 2. LeDaR method**

The interface level was deduced from the images by applying an edge detection algorithm similar to the Sobel filter. A special kernel matrix was convolved to each image of the interface, it had the property to yield matrices with high positive values in places of high vertical gradient of luminous intensity, and low negative values in the opposite case. Since the interface appeared as a bright nearly horizontal curve on a dark background, the convolved matrices presented a positive peak just below the interface and a negative peak just above. The interface in each column was thus detected as the middle point between these extremes. Instead of the vertical Sobel kernel $G_y$, the $(9 \times 3)$ kernel $G_{y9}$ was used, eq. (1). It presented the advantage of being less sensitive to noise generated by laser reflexions. A threshold system was added in order to avoid processing columns of pixels lacking lighting.

$$G_y = \begin{bmatrix} -1 & -2 & -1 \\ 0 & 0 & 0 \\ 1 & 2 & 1 \end{bmatrix}, \quad G_{y9} = \begin{bmatrix} -1 & -2 & -1 \\ \vdots & \vdots & \vdots \\ -1 & -2 & -1 \\ 0 & 0 & 0 \\ 1 & 2 & 1 \\ \vdots & \vdots & \vdots \\ 1 & 2 & 1 \end{bmatrix} \tag{1}$$

### *Verification of the LeDaR technique*

The accuracy of the LeDaR technique was verified by comparing the measurements with the analytical solution of smooth stratified flows. This presented a particular difficulty: examination of the experimental data pointed out the systematic presence of an interface level gradient (ILG), *i. e.* the measured interfaces all had a slight downward slope of about a tenth of degree. This ILG is a phenomenon described and explained by Bishop and Deshpande [9]. According to them, the variation of channel resistance in a non-established flow is balanced by a gradual variation of the interface level. The momentum balance equations for a steady-state stratified flow with ILG were derived by several researchers [10-12]. Applied to a flow with ILG between parallel plates (as sketched in fig. 3), eq. (2) is obtained:

$$\frac{\mathrm{d}h}{\mathrm{d}x} = \frac{\dfrac{\tau_\mathrm{g}}{H-h} - \dfrac{\tau_1}{h} + \tau_\mathrm{i}\left[\dfrac{1}{H-h} + \dfrac{1}{h}\right]}{\rho_1 g - \left[\dfrac{\rho_\mathrm{g} U_{mg}^2}{H-h} + \dfrac{\rho_1 U_{ml;}^2}{h}\right]} \tag{2}$$

where $\tau_\mathrm{g}$ is the wall shear stress at the top wall, $\tau_1$ – the wall shear stress at the bottom wall, and $\tau_\mathrm{i}$ – the interfacial shear stress. They are defined as $\tau = \rho\nu|\partial u/\partial y|$, with $\partial u/\partial y$ evaluated at $y = 0$, $h$ or $H$. $U_\mathrm{mg}$ and $U_\mathrm{ml}$ are the mean gas and liquid velocities, respectively.

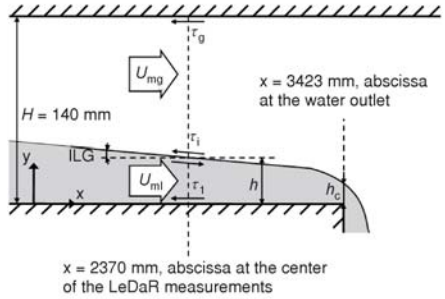


**Figure 3. Smooth stratified flow with ILG between parallel plates**

At the air outlet, the film thickness is equal to the critical thickness $h_\mathrm{c}$, which verifies $\rho_1 g - [\rho_\mathrm{g} U_{mg}^2/(H - h_\mathrm{c}) + \rho_1 U_{ml}^2/h_\mathrm{c}]$. The usual method is to evaluate $\tau_\mathrm{i}$, $\tau_\mathrm{g}$, and $\tau_1$ from empirical correlations, and to compute $\mathrm{d}h/\mathrm{d}x$ and $h$ step by step, from the outlet to any abscissa in the channel. However, these empirical correlations were established either in pipes, or for larger holdup than here (see [13] for a review). Hansen and Vested [14] proposed a different approach, valid in ducts of rectangular section and in the configuration sketched in fig. 3. They assumed that both the gas and liquid phases were in the turbulent regime, and that the Reynolds-averaged streamwise velocity followed a log law close to the walls and the interface. As a result, they expressed the streamwise velocity profile in each phase as the sum of two logarithmic functions:

$$U_1 = a_1 \ln\left(\frac{y}{h}\right) - b_1 \ln\left(1 - \frac{y}{h}\right) + c_1 \quad \text{for} \quad 0 \le y \le h \tag{3}$$

$$U_\mathrm{g} = a_\mathrm{g} \ln\left(\frac{H-y}{H-h}\right) - b_\mathrm{g} \ln\left(1 - \frac{H-y}{H-h}\right) + c_\mathrm{g} \quad \text{for} \quad h \le y \le H \tag{4}$$

Following their method, the coefficients $a_{\mathrm{g},1}$, $b_{\mathrm{g},1}$ and $c_{\mathrm{g},1}$ can be determined with conditions in the log law regions, assuming that the interface is like a moving wall of velocity $U_\mathrm{i}$:

$$U_1 = \frac{u_{\tau\mathrm{l}}}{\kappa_0} \ln\left(\frac{10 u_{\tau\mathrm{l}}\, y}{\nu_1}\right) \text{ close to the bottom wall} \tag{5}$$

$$U_1 = U_\mathrm{i} - \frac{u_{\tau\mathrm{il}}}{\kappa_0} \ln\left(\frac{10 u_{\tau\mathrm{il}}\,(h-y)}{\nu_1}\right) \text{ below the interface} \tag{6}$$

$$U_\mathrm{g} = U_\mathrm{i} + \frac{u_{\tau\mathrm{ig}}}{\kappa_0} \ln\left(\frac{10 u_{\tau\mathrm{ig}}\,(y-h)}{\nu_\mathrm{g}}\right) \text{ above the interface} \tag{7}$$

$$U_\mathrm{g} = \frac{u_{\tau\mathrm{g}}}{\kappa_0} \ln\left(\frac{10 u_{\tau\mathrm{g}}\,(H-y)}{\nu_\mathrm{g}}\right) \text{ close to the top wall} \tag{8}$$

Conditions (5) to (8) introduce the friction velocities $u_{\tau\mathrm{l},\tau\mathrm{g},\tau\mathrm{il},\tau\mathrm{ig}}$ in the calculation. They are defined as $u_\tau = (\tau/\rho)^{1/2}$, where $\tau$ is the wall or interfacial shear stress. In order to calculate the full velocity profile, additional closure equations are required:

$$U_{\mathrm{ml}} = \frac{1}{h}\int_0^h U_1 \mathrm{d}y = \frac{u_{\tau 1}}{\kappa_0}\left[\ln\left(\frac{10u_{\tau 1}h}{\nu_1}\right)-1\right]+\frac{u_{\tau i1}}{\kappa_0} \tag{9}$$

$$U_{\mathrm{mg}} = \frac{1}{H-h}\int_h^H U_{\mathrm{g}} \mathrm{d}y = \frac{u_{\tau \mathrm{g}}}{\kappa_0}\left[\ln\left(\frac{10u_{\tau \mathrm{g}}(H-h)}{\nu_{\mathrm{g}}}\right)-1\right]-\frac{u_{\tau \mathrm{ig}}}{\kappa_0} \tag{10}$$

$$\tau_{\mathrm{il}} = \tau_{\mathrm{ig}} \Rightarrow u_{\tau \mathrm{il}} = u_{\tau \mathrm{ig}}\sqrt{\frac{\rho_{\mathrm{g}}}{\rho_1}} \tag{11}$$

Equations (9) and (10) express the mean phase velocities (whose values are known) as functions of the friction velocities and film thickness. Equation (11) is the equilibrium of shear stresses at the interface, which results in an equality between friction velocities. Combined with eq. (2), the system is closed and the film thickness as well as the velocity profile can be computed iteratively at any abscissa. Furthermore, this model can be adjusted in order to solve a laminar film sheared by a turbulent gas. The principle is to describe the streamwise velocity profile in water by a sum of linear and logarithmic functions. This is done by replacing eqs. (3), (5), and (9) by eqs. (12), (13), and (14) in the described system:

$$U_1 = a_1\frac{y}{h} - b_1\ln\left(1-\frac{y}{h}\right)+c_1 \text{ for } 0 \le y \le h \tag{12}$$

$$U_1 = \frac{u_{\tau 1}^2 y}{\nu_1} \text{ close to the bottom wall} \tag{13}$$

$$U_{\mathrm{ml}} = \frac{1}{h}\int_0^h U_1 \mathrm{d}y = \frac{u_{\tau 1}^2 h}{2\nu_1}+\frac{u_{\tau \mathrm{il}}}{\kappa_0} \tag{14}$$

Both versions of this model were implemented as described in fig. 4. Predictions are shown in fig. 5; they are in reasonable agreement with experimental data. It is not possible to

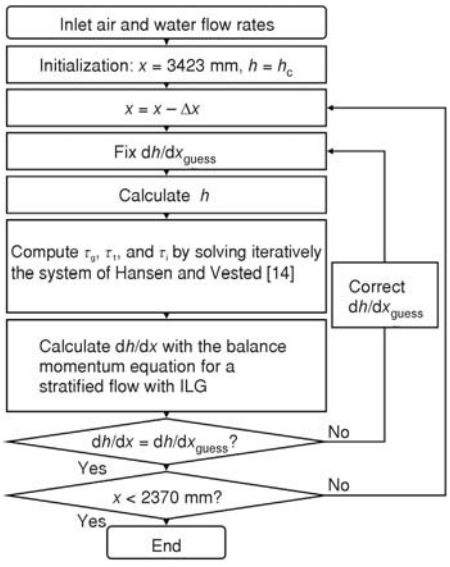


**Figure 4. Film thickness calculation flow chart**

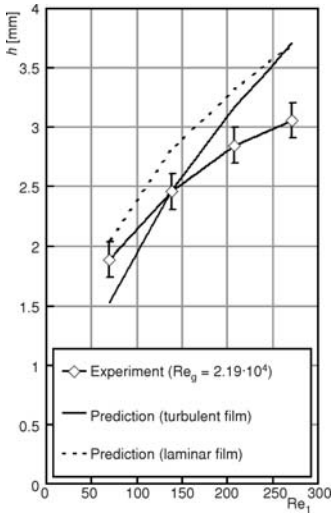


**Figure 5. Evolution of the film thickness at $x$ = 2370 mm for a smooth stratified flows, experiment and predictions**

give a ruling on the regime of the liquid film based on this work, although the absence of waves leads to think that the film is laminar. The small gap between measurements and predictions can be explained by 3-D effects not taken into account in the models. It could also come from assumptions on the shape of the velocity profile. In particular, the actual velocity profile should exhibit a flat region around the center of the gas phase, which is not the case in either version of the model.

## Experimental results and discussion

### *Flow regimes*

In this experiment, the Reynolds number based on the mean height and velocity of each phase varied from 0 to $1.16 \cdot 10^5$ in the air phase, and 69 to 271 in the water phase. Within this range, measurements were made for 24 configurations, and the flow pattern was determined visually for each run. The presence of fluorescein in the water highlighted the crests and troughs of the interface, making the characterization of the flow pattern easier. At null and low gas Reynolds number, the water film remained smooth; further increase in air velocity triggered the wavy stratified flow pattern. At the lowest liquid Reynolds number, 2-D waves were visible, but quickly broke into 3-D waves. The fan was not powerful enough to reach the Kelvin-Helmholtz or roll wave flow pattern that appears at the onset of atomization.

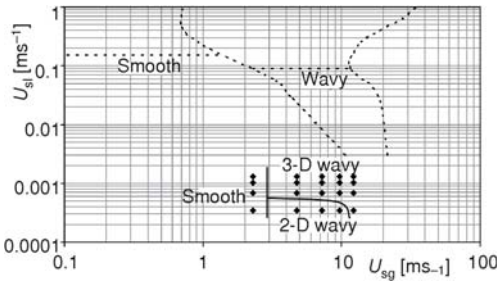


**Figure 6. Map of Mandhane, *et al*. [15] with transitions in dashed lines. Approximate transitions of this experiment are indicated with solid lines**

Figure 6 plots the runs on the flow map of Mandhane *et al*. [15], except for those at null gas Reynolds number. The agreement between the observed patterns and the flow map is poor, partly because the authors heavily relied on pipes of round section to establish their map. It is also known that the transition from smooth to wavy stratified is sensitive to inlet conditions and to the presence of an ILG (see [9]), it is thus difficult to predict.

### *Statistic analysis*

The LeDaR measurements gave 100 mm long sample records of the interface, and 100 images were taken for each runs. This yielded about 183000 points per run, which were used to calculate estimates of the mean film thickness $\bar{h}$ and RMS of the interfacial fluctuations $h_{\mathrm{RMS}}$. Results are presented in fig. 7 and 8. Quite logically, $\bar{h}$ is a monotonic function of the liquid Reynolds number and decreases quasi linearly with increasing gas Reynolds number. $h_{\mathrm{RMS}}$ also is a monotonic function of the liquid Reynolds number, which reflects that increasing the water flow rate results in a larger degree of freedom of the interface fluctuations. On the

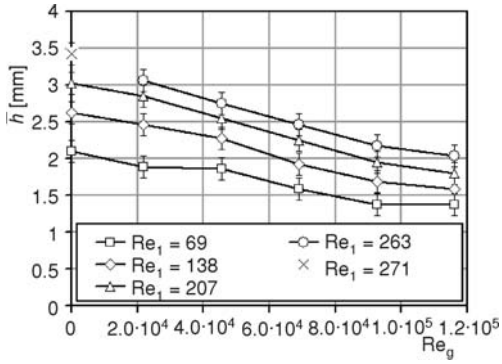


**Figure 7. Evolution of the mean film thickness**

other hand, it seems that $h_{RMS}$ reaches a threshold value at high gas Reynolds number. These results only partially agree with those of Lioumbas, *et al*. [3] who reported a peak of $h_{RMS}$ at the onset of the 2-D wavy stratified flow pattern. The fact that we did not observe this peak may come from an insufficient number of runs in the investigated range, or from the difference in experimental conditions such as pipe section, inclination and phase velocities.

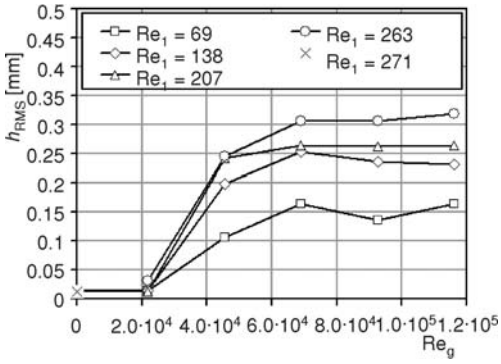


**Figure 8. Evolution of the RMS film thickness**

### *Spectral analysis of the interface*

For each run with a wavy interface, we computed the power spectrum (PS) of the signal formed by lining up all of the LeDaR sample records. The so-called "Welch's Overlapped Segmented Average" method [16] was used; results are given in figs. 9 to 12. 2-D wavy stratified flows always produce a broad peak, from which the dominant spatial frequency is extracted. As seen in tab. 1, this frequency increases with the gas Reynolds number. 3-D wavy stratified flows

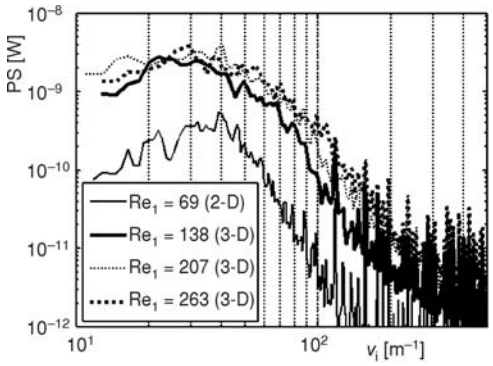


**Figure 9. PS of the interface for $Re_g = 4.54 \cdot 10^4$**

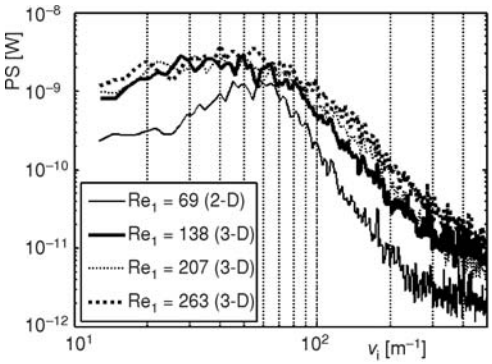


**Figure 10. PS of the interface for $Re_g = 6.90 \cdot 10^4$**

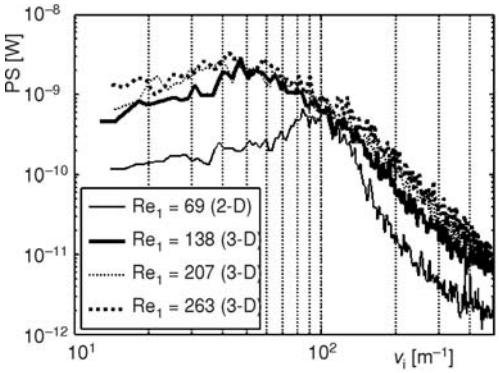


**Figure 11. PS of the interface for $Re_g = 9.26 \cdot 10^4$**

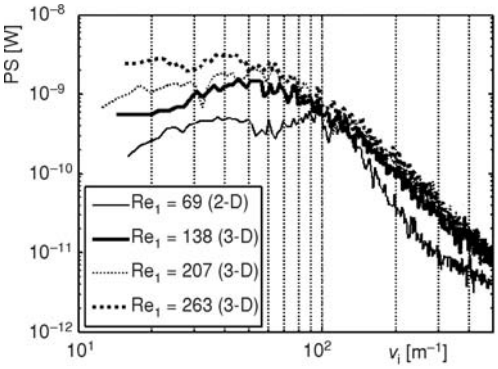


**Figure 12. PS of the interface for $Re_g = 1.16 \cdot 10^5$**

involve a wider range of wavelengths and produce flatter PS. The pattern obtained at $Re_l = 69$ and $Re_g = 1.16 \cdot 10^5$ shown in fig. 12 can be considered as the onset of 3-D waves: a peak of energy is still visible around $\nu_i = 100$ m$^{-1}$, but at the same time an increase of energy appears at lower frequencies.

**Table 1. Evaluation of the dominant spatial frequency and associated wavelength in 2-D wavy stratified flow patterns**

| Run | Dominant spatial frequency [m$^{-1}$] | Wavelength [mm] |
|---|---|---|
| $Re_l = 69$, $Re_g = 4.54 \cdot 10^4$ | 40 | 25 |
| $Re_l = 69$, $Re_g = 6.90 \cdot 10^4$ | 65 | 15.38 |
| $Re_l = 69$, $Re_g = 9.26 \cdot 10^4$ | 85 | 11.76 |

The PS gave us a global information about the interface, nevertheless a better understanding of the simultaneous transport of high and low frequency waves came with a direct study of the LeDaR measurements. Four mechanisms were identified, each of them is illustrated in figs. 13 to 16.

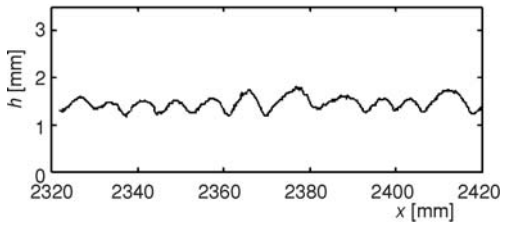


**Figure 13. Wavelength smoothly varying around a dominant value ($Re_l = 69$, $Re_g = 9.26 \cdot 10^4$)**

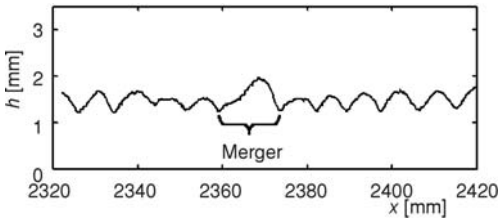


**Figure 14. Merger of waves ($Re_l = 69$, $Re_g = 9.26 \cdot 10^4$)**

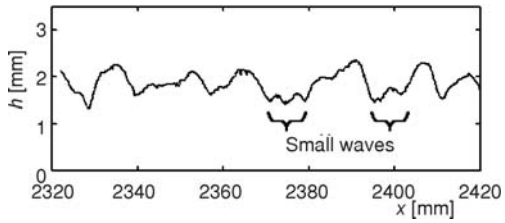


**Figure 15. Waves with non-coinciding midspan plane ($Re_l = 138$, $Re_g = 9.26 \cdot 10^4$)**

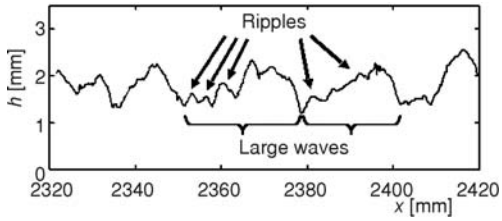


**Figure 16. Ripples riding larger waves ($Re_l = 207$, $Re_g = 1.16 \cdot 10^5$)**

– In 2-D wavy stratified flows, the wavelength is not constant but smoothly varies around a dominant value. This small oscillation seems random and therefore could be due to turbulent fluctuations in the velocity field. It explains why the PS of 2-D wavy stratified flows present a broad peak instead of a sharp one.
– Two waves that follow each other can merge into a larger one. This mechanism occasionally occurs in both 2-D and 3-D wavy stratified flows, and is another factor of spreading of the spatial frequency bandwidth.

– The spanwise dimension of 3-D waves is obviously smaller than the width of the channel. In some of the 3-D wavy stratified flows, the waves are approximately of the same dimensions but their midspan planes are not coinciding, so that the measurements reveal small waves stuck between large ones.
– One or more ripples can move on the crest of a larger wave, or in the trough between two large waves. This phenomenon occurs more often when increasing the gas Reynolds number.

A final observation is made from the LeDaR measurement: all the sample records show that the waves are limited to the upper layer of the film. Even for $\overline{h} \approx 1.5$ mm, there is always an undisturbed substrate of at least 1 mm. This suggests that, even for a very disturbed interface, there exist a near-wall zone in the film where transfers by conduction may be predominant.

## Conclusions

The interfacial characteristics of a horizontal stratified air-water flow were investigated experimentally in a duct of 200 × 400 mm section and with a small holdup. The interface was visualized and measured in the midspan plane with the LeDaR technique. This particular method was first assessed for smooth stratified flows, it then revealed an ILG due to the relatively large dimensions of the channel. It was also found that the $h_{RMS}$ was a monotonic function of the liquid Reynolds number, but seemed to reach a limit value at high gas Reynolds number. A spectral analysis showed that both the 2-D and 3-D wavy stratified flow patterns had a large spatial frequency bandwidth, although a dominant frequency could be found for 2-D waves. With the LeDaR sample records, four mechanisms were found to contribute to the spreading of the spatial frequency bandwidth. When they occur simultaneously, the interface results in a seemingly disorganized signal. As a consequence, the understanding of heat and mass transfer through this kind of wavy films could benefit from an accurate CFD modeling. In this respect, the results of this paper could very well be used as experimental reference for validation purpose.

## Acknowledgment

The authors are grateful for the financial support of the Robert Bosch group.

## Nomenclature

$g$ – gravitational acceleration, [ms$^{-2}$]
$H$ – height of the two-phase flow channel (= 140 mm)
$h$ – liquid film thickness, [mm]
$\overline{h}$ – mean value of the liquid film thickness, [mm]
$h_c$ – critical film thickness at the outlet of the channel, [mm]
$h_{RMS}$ – RMS value of the liquid film thickness fluctuation, [mm]
Re – Reynolds number in a phase ($= U_{mg}(H - \overline{h})/\nu_g$ in the gas phase; $= U_{ml}\overline{h}/\nu_l$ in the liquid phase), [–]
$U_m$ – mean velocity of a phase, [ms$^{-1}$]
$U_s$ – superficial velocity of a phase ($= (1 - \alpha)U_{mg}$ in the gas phase; $= \alpha U_{ml}$ in the liquid phase), [ms$^{-1}$]
$U(x, y)$ – Reynolds-averaged streamwise velocity, [ms$^{-1}$]
$u_\tau$ – friction velocity at a wall or at the interface, [ms$^{-1}$]
$\nu_i$ – spatial frequency of interfacial waves, [m$^{-1}$]

### *Greek symbols*

$\alpha$ – holdup, *i.e.* liquid volume fraction in a section of the channel, [–]
$\kappa_0$ – von Karman constant (= 0.41)
$\nu$ – kinematic viscosity, [m$^2$s$^{-1}$]
$\rho$ – density, [kgm$^{-3}$]
$\tau$ – wall or interfacial shear stress, [Pa]

### *Subscripts*

g – in the gas phase
l – in the liquid phase
i – at the interface
ig – at the interface, on the gas side
il – at the interface, on the liquid side

## References

[1] Hagiwara, Y., *et al*., Simultaneous Measurement of Liquid Film Thickness, Wall Shear Stress and Gas Flow Turbulence of Horizontal Wavy Two-Phase Flow, *International Journal of Multiphase Flow, 15* (1989), 3, pp. 421-431
[2] Paras, S. V., *et al.*, Liquid Layer Characteristics in Stratified-Atomization Flow, *International Journal of Multiphase Flow, 20* (1994), 5, pp. 939-956
[3] Lioumbas, J. S., *et al*., Co-Current Stratified Gas-Liquid Down Flow – Influence of the Liquid Flow Field on Interfacial Structure, *International Journal of Multiphase Flow, 31* (2005), 8, pp. 869-896
[4] Akai, M., *et al*., A Co-Current Stratified Air-Mercury Flow with Wavy Interface, *International Journal of Multiphase Flow, 6* (1980), 3, pp. 173-190
[5] Zouana, A., Study of Mass Transfers at the Interface of a Laminar, Non-Established Liquid Film (in French), Ph. D. thesis, University of Poitiers, Poitiers, France, 1988
[6] Planquart, P., *et al*., Real Time Optical Detection and Characterisation of Water Model Free Surfaces – Application to the Study of the Mold, *Proceedings*, 4th European Continuous Casting Conference, Birmingham, UK, 2002
[7] Toth, B., *et al.*, Dynamic Measurements of the Shape of a Free Surface (in French), *Proceedings*, 9th Congress Francophone on Laser Technique, Toulouse, France, 2006
[8] Toth, B., Two-Phase Flow Investigation in a Cold-Gas Solid Rocket Motor Model through the Study of the Slag Accumulation Process, Ph. D. thesis, Free University of Bruxelles, Brussels, Belgium, 2008
[9] Bishop, A. A., Deshpande, S. D., Interfacial Level Gradient Effects in Horizontal Newtonian Liquid-Gas Stratified Flow-I, *International Journal of Multiphase Flow, 12* (1986), 6, pp. 957-975
[10] Bishop, A. A., Deshpande, S. D., A Criterion to Determine Uniform and Non-Uniform Stratified Liquid-Gas Flow through Horizontal Tubes, *International Communications in Heat and Mass Transfer, 13* (1986), 2, pp. 209-217
[11] Taitel, Y., Dukler, A. E., Effect of Pipe Length on the Transition Boundaries for High-Viscosity Liquids, *International Journal of Multiphase Flow, 13* (1987), 4, pp. 577-581
[12] Sadatomi, M., *et al.*, Prediction of Liquid Level Distribution in Horizontal Gas-Liquid Stratified Flows with Interfacial Level Gradient, *International Journal of Multiphase Flow, 19* (1993), 6, pp. 987-997
[13] Ottens, M., *et al*., Correlations Predicting Liquid Hold-Up and Pressure Gradient in Steady State (Nearly) Horizontal Co-Current Gas-Liquid Pipe Flow, *Transactions of the Institution of Chemical Engineers, 79* (2001), 5, pp. 581-592
[14] Hansen, E. A., Vested, H. J., Liquid Hold-Up, Pressure Drop, and Velocity Profiles in Steady Uniform Stratified Flow, *Journal of Energy Resources Technology, 113* (1991), 2, pp. 87-93
[15] Mandhane, J. M., *et al.*, A Flow Pattern Map for Gas-Liquid Flow in Horizontal Pipes, *International Journal of Multiphase Flow, 1* (1974), 4, pp. 537-553
[16] Welch, P. D., The Use of FFT for the Estimation of Power Spectra: a Method Based on Time Averaging Over Short, Modified Periodograms, *IEEE Transactions of Audio and Electroacoustics, 15* (1967), 2, pp. 70-73

Paper submitted: June 2, 2012
Paper revised: September 9, 2012
Paper accepted: October 17, 2012